Influence of iron substitution on structural, magnetic, and magnetocaloric properties of Tb_2Fe_1_7_−_xAl_x compounds synthesized by arc melting

S. Charfeddine, I. Souid, H. Jaballah, Lotfi Bessais, A. Korchef

Influence of iron substitution on structural, magnetic, and magnetocaloric properties of $Tb_2Fe_{17-x}Al_x$ compounds synthesized by arc melting

S. Charfeddine,[1,2] I. Souid,[3] H. Jaballah,[4,2] L. Bessais,[2] and A. Korchef *[3,1]

[1] *LVMU, Centre National de Recherches en Sciences des Matériaux, Technopole de Borj-Cédria, BP 73 Soliman 8027, Tunisia*
[2] *Univ Paris Est Creteil, CNRS, ICMPE, UMR 7182, 2 rue Henri Dunant, F-94320 Thiais, France*
[3] *Joint Programs, College of Science, King Khalid University (KKU), P.O. Box 9004, 61413 Abha, Saudi Arabia*
[4] *Université de Tunis El Manar, Faculté des Sciences de Tunis, Laboratoire Matériaux Organisation et Propriétés, Tunis 2092, Tunisia.*

(Dated: October 8, 2023)

ABSTRACT

In the present work, the structure and magnetic and magnetocaloric properties of the $Tb_2Fe_{17-x}Al_x$ compounds with $x = 0, 0.25, 0.5, 0.75$, and 1 were studied. These compounds were synthesized by arc furnace without subsequent annealing. Their crystal structure is a Th_2Ni_{17} hexagonal structure with a $P6_3/mmc$ space group. The Rietveld refinement of the X-ray diffractograms allowed for determining the structural parameter variations with different amounts of aluminum. Lattice parameters and the unit cell volume increase with aluminum amounts while the c/a ratio remains nearly constant. The $Tb_2Fe_{17-x}Al_x$ compounds exhibit a second-order magnetic phase transition from a ferromagnetic state to a paramagnetic state. The Curie temperature (T_C) increases with the aluminum content, the observed effect is due to the magnetovolumic effect. The saturation magnetization (M_S) decreases with the increase of Al content. Magnetic entropy and relative cooling power (RCP) decrease as the aluminum content increases. $Tb_2Fe_{17-x}Al_x$ compounds have a moderate magnetocaloric effect and a tunable operating temperature interval.

PACS numbers: 75.50.Bb, 75.50.Tt, 76.80.+y
Keywords: Rare-earth intermetallics; Magnetic properties; Diffraction; Magnetic refrigeration.

I. INTRODUCTION

Intermetallic compounds have been a subject of considerable interest in the field of materials science and engineering, due to their distinct crystal structure and exceptional physical and mechanical properties. Ni_3Al, Ni_3Fe, and Nb_3Sn are intermetallic compounds that find wide usage in high-temperature industrial settings due to their unique physical properties, which are more fascinating than those of ceramics and superalloys. For instance, intermetallics exhibit a lower brittleness than ceramics due to their metallic bonding, and they possess a higher strength than superalloys because of the strong bonds between atoms. These properties have been established in previous studies [1, 2]. The exceptional magnetic properties of intermetallics based on rare earth-transition metal (R-T), such as high-performance permanent magnets, high-density magnetic recording, and magnetic refrigeration, make them highly valued materials [3–7]. As a result, there has been extensive research into R-Fe intermetallics, with the aim of developing novel magnetic devices [4, 8–17]. Several R-Fe intermetallic compounds, including RFe_2, RFe_3, $R6Fe_{23}$, and R_2Fe_{17} (where R can be Tb or Dy), have been confirmed to exist through phase diagram studies [18–21]. Among all binary combinations of type R-T, R_2T_{17} intermetallics show promising potential in magnetic materials and magnetic refrigeration applications. R_2Fe_{17} compounds exhibit one of the highest saturation magnetization after RM_{12} alloys [22]. However, these compounds possess planar anisotropy and low Curie temperature [23–26], which limit their industrial performance. The magnetocrystalline anisotropy of R_2Fe_{17} compounds results from the combination of the anisotropies of the rare earth and iron elements, with the latter usually dominating at high temperatures ($T < T_C$), while the former prevails at low temperatures. The low Curie temperature arises from the interatomic distances between Fe atoms, which fall below the critical value of 2.45 Å, required for ferromagnetic exchange interactions. To address these challenges, partial substitutions of iron with an element that increases the Curie temperature by the magnetovolume effect can be made. It has been demonstrated that R_2Fe_{17} compounds can tolerate moderate amounts of nitrogen or carbon without altering their structure, although their planar anisotropy changes to uniaxial anisotropy [27]. Furthermore, partial substitution of iron by Al [9], Mn [28], Cr [29], or Si [30], or replacement of the rare earth element by another, promotes the application of these compounds in various technological domains.

The compound Tb_2Fe_{17} consists of two crystal structures, namely the rhombohedral Tb_2Fe_{17} with a $R\bar{3}m$ space group and the hexagonal Tb_2Fe_{17} with a $P6_3/mmc$ space group, both based on the $CaCu_5$-type structure [18, 19, 21, 31]. Studies have revealed that the hexagonal structure dominates when the Tb/Fe molar ratio is 2/17

(10.5 or 9.5 at % Tb), whereas the rhombohedral structure becomes more prevalent at higher Tb content of 11.5 at % [32]. Due to its iron-rich composition, the Tb_2Fe_{17} system provides a suitable platform for investigating both $3d$ and $4f$ magnetism, as well as their interplay.

The potential for producing cold makes magnetic refrigeration a highly attractive technology. This cooling method is based on the magnetocaloric effect, which is exhibited in most magnetic compounds, including intermetallic compounds such as R_2Fe_{17}. The magnetocaloric effect is an intrinsic property of paramagnetic and ferromagnetic materials, causing them to experience a temperature increase when subjected to a fluctuation in magnetic field in adiabatic conditions, and a cooling effect upon demagnetization. This phenomenon arises from the coupling between the magnetic moments of localized or itinerant electrons in a compound with a magnetic field, which alters the magnetic part of the total entropy (ΔS). Note that the total entropy (ΔS) at constant pressure has three contributions: magnetic, electronic, and lattice. The change in magnetic entropy under adiabatic conditions can be determined from the experimental data on isothermal magnetization using the Maxwell relation, as described in [33].

In this investigation, we effectively fabricated the hexagonal phase of the $Tb_2Fe_{17-x}Al_x$ materials with x varying from 0 to 1, using arc melting without subsequent annealing. Our primary objective was to assess how substituting aluminum for iron influenced the crystal structure and magnetic properties, including the magnetocaloric effect, in the $Tb_2Fe_{17-x}Al_x$ system. To identify the phases present in the samples, we performed a comprehensive X-ray diffraction analysis and conducted Rietveld refinement. The magnetic measurements were focused on highlighting the order of the magnetic transition phase and magnetocaloric effect.

II. EXPERIMENTAL METHODS

Tb_2Fe_{17} starting composition ingots were synthesized from high-purity Fe (99.99 %) and Tb (99.98 %) elements using the conventional arc-melting technique. To ensure homogeneity, the samples underwent a series of three meltings at increasing generator intensity levels (60 A, 70 A, 80 A). The resulting ingots were then fragmented in an inert argon atmosphere within a glove box. To produce a single-phase material, multiple samples of the Tb_2Fe_{17} binary compound were synthesized through arc-melting with varying Tb content. A single phase with 10.5 at % Tb was obtained without the requirement of additional heat treatment, simply through the melting process. Thereafter, iron was partially substituted by high-purity aluminum (Al 99.99 %), and the polycrystalline $Tb_2Fe_{17-x}Al_x$ samples ($x = 0.25, 0.5, 0.75$ and 1) were prepared by arc melting under a high purity argon following the same steps as for the preparation of the material with the starting composition Tb_2Fe_{17}.

X-ray diffraction was performed using a Brucker diffractometer with a Cu radiation source and an internal Si standard, ensuring a unit cell accuracy of $\pm 1 \cdot 10^{-3}$ Å. The XRD patterns were obtained at room temperature with a step size of 0.02° and a counting time of 192 seconds per step over a scanning range of $2\theta = 20 - 90°$. The data analysis was conducted through the Rietveld method as implemented in the FullProf computer code, which accounted for the Thompson-Cox-Hastings peak line profile and allowed for the refinement of multiple phases coexisting in the sample [34, 35].

The magnetic measurements were conducted using a DSM-8 MANICS differential sample magnetosusceptometer, which operates on a similar principle as a Faraday balance. the measured samples were sealed under a secondary vacuum to avoid oxidation by heating during the measurement.

III. RESULTS AND DISCUSSION

A. Structure analysis

The Tb_2Fe_{17} compound is a bulk material that has a hexagonal Th_2Ni_{17}-type structure with a $P6_3/mmc$ space group. This structure consists of Fe atoms occupying four crystallographic sites ($12k, 12j, 6g, 4f$ in the Wyckoff site position) and Tb atoms occupying two crystallographic sites (2c and 2b). The hexagonal structure is derived from the $CaCu_5$-type structure through the substitution of a pair of Fe-Fe dumbbells for every third Tb atom. This information is reported by [24] Fig. 1 shows the X-ray diffraction patterns of $Tb_2Fe_{17-x}Al_x$ polycrystalline samples with different aluminum contents ($x = 0, 0.25, 0.5, 0.75$, and 1) were obtained by arc melting. All samples showed a pure phase with a hexagonal structure having a space group of $P6_3/mmc$. To investigate the effect of aluminum content on the structural parameters of the $Tb_2Fe_{17-x}Al_x$ compounds, we conducted Rietveld refinement of the X-ray diffraction diagrams, assuming that the aluminum atoms occupy the $4f$ site. According to the calculation of the Wigner-Seitz cell volumes, the $4f$ site has the largest volume among the crystallographic sites. To confirm that aluminum preferentially occupies the $4f$ site, we performed X-ray diffraction refinement by placing the aluminum atoms at different crystallographic sites ($12k, 12j, 6g, 4f$), and evaluated the goodness-of-fit indicator R_B using the equation:

$$R_B = 100 \frac{\sum_K |I_K(O) - I_K(C)|}{\sum_K I_K(O)}$$

The computed Bragg intensity is denoted as $I_K(C)$ while the measured Bragg intensity is represented by $I_K(O)$. In Fig. 2, it can be observed that the indicator R_B varies for the different crystallographic aluminum sites, with

the lowest value obtained for the $4f$ site. Hence, based on these results, it can be concluded that site $4f$ is the preferred site for aluminum. A similar observation was made for $Er_2Fe_{17-x}Al_x$ intermetallic compounds where aluminum atoms were found to preferably occupy the $4f$ sites [36].

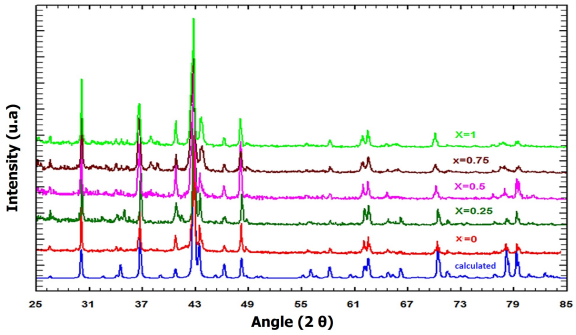

Figure 1. XRD diagrams of $Tb_2Fe_{17-x}Al_x$ ($x = 0, 0.25, 0.5, 0.75, 1$).

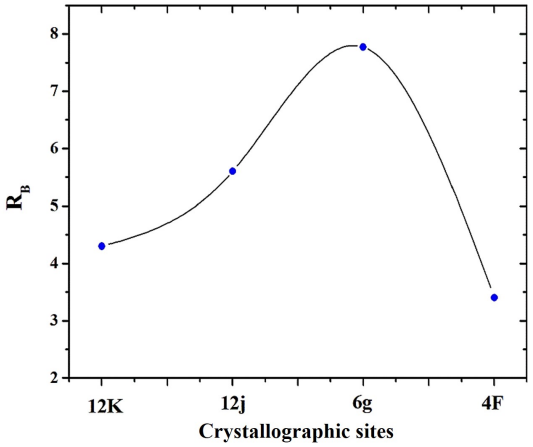

Figure 2. The "goodness-of-fit" indicator R_B variation for different crystallographic aluminum sites.

In the Fig. 3, we can see the Rietveld refinements of the X-ray diffraction (XRD) diagrams for the $Tb_2Fe_{17-x}Al_x$ compounds produced by arc melting. The positions of the Bragg reflections are denoted by green vertical bars, while the blue solid line shows the differences between the observed and calculated intensities. The calculated refinement results can be found in Table I. The samples produced are pure in phase, except for the two samples with $x = 0.75$ and $x = 1$, where an extra peak appears around $2\theta = 38°$. This peak could be attributed to either an excess of aluminum, in which case it corresponds to the plane (111) of the cubic centered faces phase of aluminum, or to the onset of the rhombohedral phase of the structure Th_2Zn_{17}, in which case it corresponds to the plane (024). Previous studies by Mishra et al. [37] have shown that for $x \leq 1$, $Tb_2Fe_{17-x}Al_x$ compounds crystallize in the hexagonal phase Th_2Ni_{17}, and for $x \geq 1$, they crystallize in the rhombohedral phase Th_2Zn_{17}.

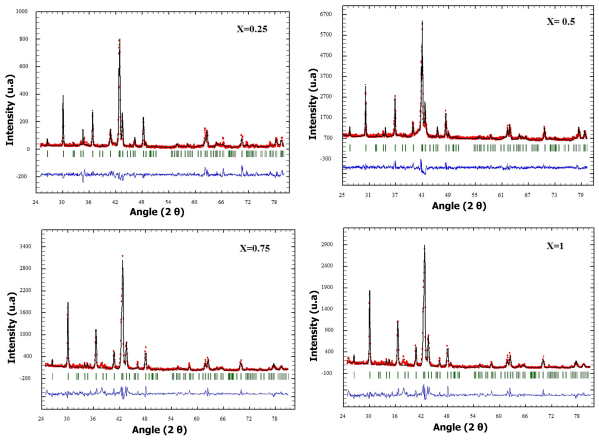

Figure 3. Observed (dots) and calculated (solid line) XRD patterns for the $Tb_2Fe_{17-x}Al_x$ ($x = 0.25, 0.5, 0.75, 1$) compounds. The Bragg positions are represented by the vertical bars. The experimental-simulated difference is shown at the bottom of the figure.

Table I. a and c unit cell parameters, R_B, χ^2 factors, and atomic positions from Rietveld refinement of $Tb_2Fe_{17-x}Al_x$ ($x = 0.25, 0.5, 0.75, 1$).

	$x = 0$	$x = 0.25$	$x = 0.5$	$x = 0.75$	$x = 1$
$a(Å)$	8.4583(4)	8. 4761(1)	8.4947(2)	8.5131 (4)	8.5313(5)
$c(Å)$	8.3005(4)	8.3197(3)	8.3390(4)	8.3585(7)	8.3775(8)
c/a	0.983	0.98	0.98	0.98	0.98
$V(Å^3)$	514.2	516	519	521	523
x $12k$	0.1667(1)	0.1681(1)	0.1683(1)	0.1685(1)	0.1687(1)
x $12j$	0.3520(3)	0.3420(2)	0.3421(1)	0.3422(2)	0.3420(3)
y $12j$	0.3218(2)	0.3218(2)	0.3218(2)	0.3218(2)	0.3218(1)
z $4f$	0.6268(2)	0.6290(2)	0.6307 (3)	0.6341(1)	0.6418(2)
χ^2	4.4	3.4	3.6	2.7	3.1
R_B	6. 87	4.2	5.1	4.8	7.2

The changes in the cell parameters a and c, as well as the unit cell volumes of $Tb_2Fe_{17-x}Al_x$ compounds with varying x values (ranging from 0 to 1), are depicted in the Fig. 4. As the aluminum content increases, there is a continuous rise in cell parameters and volume. For instance, the unit cell volume increases from 514.2 $Å^3$ to 523 $Å^3$ as x goes from 0 to 1. This increase in cell volume can be attributed to the substitution of iron by aluminum, since the atomic radius of aluminum (= 1.43 Å) is marginally higher than that of iron (= 1.26 Å).

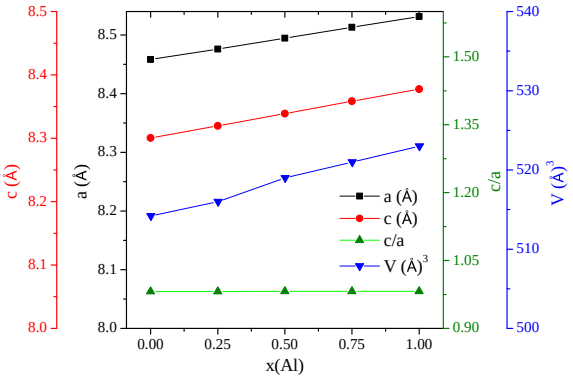

Figure 4. Cell parameters and cell volume versus aluminum content.($x = 0, 0.25, 0.5, 0.75, 1$).

B. Intrinsic magnetic properties

We conducted a systematic measurement of the thermo-magnetic curves for various $Tb_2Fe_{17-x}Al_x$ compounds with x ranging from 0 to 1 to determine their Curie temperature. The Curie temperature values were determined by estimating the minimum of the temperature derivative of the magnetization, dM/dT, versus temperature. Two thermo-magnetic curves of the ternary compounds $Tb_2Fe_{17-x}Al_x$ were presented in Fig. 5, one with x=0.25 (corresponding to the compound $Tb_2Fe_{16.75}Al_{0.25}$) and the other with the maximum value x=1 (corresponding to the compound $Tb_2Fe_{16}Al$). Both curves show a single magnetic transition from the ferromagnetic to the paramagnetic state, and the Curie temperature increases as the aluminum content increases. For instance, the Curie temperature increases from 412 K for $x = 0$ to 448 K for $x = 1$.

Typically, the Curie temperature is controlled by the exchange interactions in intermetallic compounds consisting of a transition metal and a rare earth atom. Such interactions can be classified into three types:

- The exchange energy between the transition metal atoms ($3d - 3d$).
- The exchange energy between the rare earth atoms ($4f - 4f$).
- The exchange energy between the transition metal atom and rare earth one ($4f - 3d$).

In the case of a non-magnetic rare earth element in an R-M system, the $4f - 4f$ and $3d - 4f$ exchanges can be disregarded, leaving only the $3d-3d$ exchange interaction that contributes to the Curie temperature. Conversely, in the presence of a magnetic rare earth atom, both exchange energy terms must be considered. It is worth noting that the $4f - 4f$ exchange is the weakest of the three configurations and can be considered negligible. Within intermetallics, there exist two types of exchange interactions, namely positive and negative, which depend on the distance between transition metal atom pairs. If this distance is greater than a critical value, the exchange interactions are positive, while if it is less than the critical distance, the interactions are negative [38, 39].

The critical temperature (T_C) of R_2Fe_{17} intermetallic materials can be influenced by various parameters. Specifically, T_C is determined by magnetic exchange energies $aFe - Fe$ and a_{R-Fe}, where the strength of a_{R-Fe} relies on the rare-earth de Gennes factor. The rise in T_C is influenced by several crucial factors. One of them is the electronic effect. Bessais *et al.* [40] demonstrated that as the Co content increases in $Sm_2Fe_{17-x}Co_x$, the hyperfine field increases due to the asymmetric filling of the $3d$ band by the additional electron of the Co atom, resulting in the rise of core electron polarization. Another crucial factor that contributes to the increase in T_C is the magnetovolumic effect. The critical distance in R_2Fe_{17}, where the exchange interaction becomes negative, is approximately 2.45 Å[41]. According to the Néel Slater curve, a slight increase in the Fe-Fe distances, such as the $6c-6c$, $9d - 18f$, $18f - 18f$, $18h - 18h$, and $18f - 18h$ pairs that are around the critical distance, leads to a substantial increase in $JFe - Fe$ exchange interactions, which ultimately leads to an increase in the Curie point value.

Fig. 6 displays how the Curie temperature of $Tb_2Fe_{17-x}Al_x$ compounds changes as the aluminum content increases. A marked increase in T_C can be seen with the addition of aluminum. The cause of this rise in T_C is attributed to the positive reinforcement of exchange interactions. The increase in Fe-Fe distances due to the unit cell volume expansion during iron substitution causes the strengthening of the exchange interactions $3d - 3d$ during aluminum substitution which contributes to this effect. Therefore, the increase of T_C with Al content may be due to the size effect caused by Al substitution, since the substitution of Al for Fe at the $4f$ site may reduce the negative exchange interaction. Mishra et al. [37] and Guetari et al. [9] obtained similar results.

fig. 7 displays the magnetization isotherm curves as a function of the magnetic field measured under the applied magnetic field and temperatures varying around the Curie temperature of each compound. The obtained curves indicate that the magnetization decreases upon the substitution of iron with aluminum, as aluminum is paramagnetic with a relative permeability close to 1. Moreover, the magnetization is influenced by the environment and the distance between the iron atoms and their first neighboring atoms. Thus, if other iron atoms surround the iron, there is an increase in magnetization, otherwise, if the iron is surrounded by a rare earth or another atom like aluminum, there is a reduction in magnetization. Above the Curie temperature, the compounds studied are paramagnetic, so the magnetization increases slowly with the applied magnetic field. However, below T_C, the magnetization isotherm curves of the compounds studied show a ferromagnetic behavior characterized by

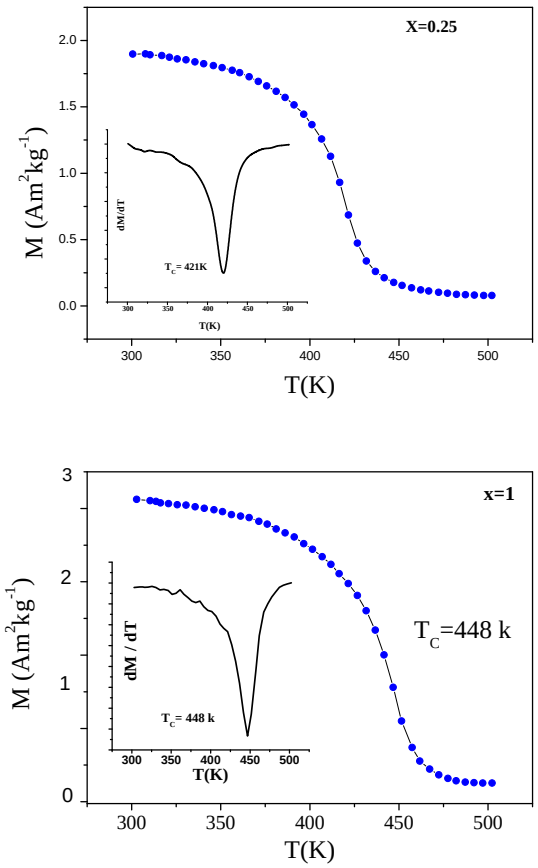

Figure 5. Temperature dependence of magnetization of $Tb_2Fe_{17-x}Al_x$ (x=0.25 and x=1) under weak applied magnetic field.

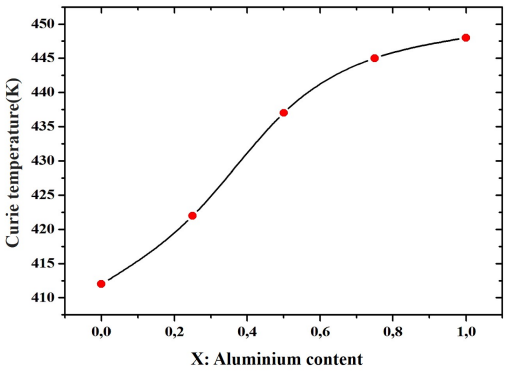

Figure 6. T_C versus Al content (x) of $Tb_2Fe_{17-x}Al_x$ compounds

a significant increase in magnetization with the applied magnetic field. Also, it is worth noticing that the magnetization increases with decreasing temperature for a given applied field.

In order to determine the values of the saturation magnetizations for the different compounds the saturation

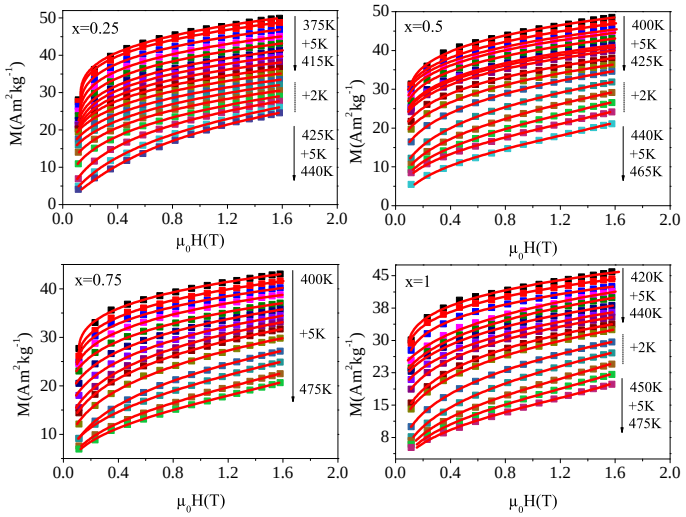

Figure 7. Isotherm magnetization curves, $M(H)$, for $Tb_2Fe_{17-x}Al_x$ compounds measured at different temperatures around the Curie temperature for magnetic fields between 0 and 1.5 T. the symbols represent the experimental magnetization and the solid red lines represent the fit curve according to the Landau model

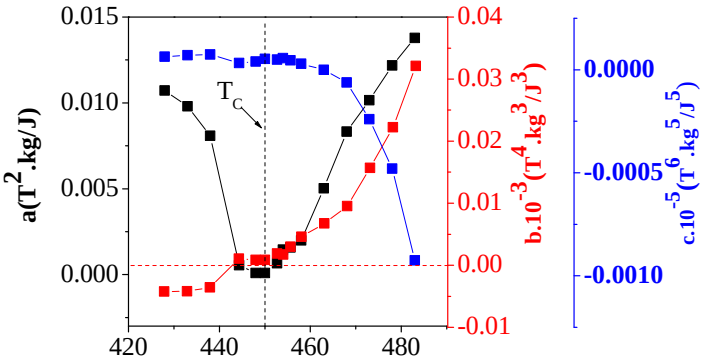

Figure 8. Landau parameters $c(T)$ vs temperature around the T_C, for $Tb_2Fe_{16}Al_1$ compounds calculated at different temperatures around the Curie.

approach law was used [42–44]. The values of M_S are presented in Tab. II, which groups together the magnetic results of the different compounds.The saturation magnetization M_S decreases when aluminum content increases. The decrease of M_S is mainly related to the magnetic dilution, through the substitution of the iron (Fe) atom, which possesses a high magnetic moment, with a quasi-non-magnetic atom (Al). Comparable results were depicted for $Pr_2Fe_{17-x}Al_x$ [9] and $Nd_2Fe_{17-x}Ga_x$ [45].

Assessing the magnetocaloric materials requires an evaluation of the magnetic phase transition's order,

which indicates the reversibility of the magnetocaloric effect. Two approaches were employed in this research to determine the phase transition order: one method based on Arrott's plots and another based on Landau's phenomenological theory. The Landau model was utilized in this section to determine the phase transition type. The magnetic free energy was expressed as a function of temperature in the vicinity of the critical temperature (T_C) while neglecting higher-order magnetization terms to characterize the magnetic phase transition order. The magnetic free energy (F) was mathematically defined as a function of the total magnetization in a particular format.

$$F = \frac{1}{2}a(T)M^2 + \frac{1}{4}b(T)M^4 + \frac{1}{6}c(T)M^6 - \mu_0 MH$$

We apply the equilibrium condition for the free energy

$$\frac{dF}{dM} = 0$$

we obtain:

$$\mu_0 H = a(T)M + b(T)M^3 + c(T)M^5$$

By plotting the magnetization M against the magnetic field $\mu_0 H$, the Landau parameters $a(T)$, $b(T)$, and $c(T)$ can be determined. The coefficients $a(T)$ and $c(T)$ are always positive, and T_C can be identified as the minimum point of $a(T)$. However, the sign of $b(T)$ can be positive, zero, or negative, and can indicate whether the magnetic transition is a first-order or second-order phase transition. In Fig. 7 the red solid line demonstrates good agreement between the experimental data and the Landau model for all compositions $Tb_2Fe_{17-x}Al_x$. As an example Fig. 8 presents the evolution of Landau parameters for the composition with $x = 1$, the Landau coefficient $b(T_C)$ is positive, which suggests that the transition from the ferromagnetic to paramagnetic state is a second-order phase transition. The minimum point of $a(T)$ corresponds well with the Curie temperature values obtained from thermomagnetic measurements.

The method of Arrott plots has several advantages, we can mention:

- We can determine the value of the Curie temperature, by identifying the critical isotherm which is a linear line passing through the origin.
- Based on Banerjee's criterion, it is possible to determine the order of the magnetic transition, in fact, if the isotherms drawn in the form $M^2 = f(H/M)$ have positive slopes so the transition is second-order, on the other hand, if the isotherms have negative slopes and have a similar shape of the letter S the transition is classified as first-order. all the plots presented in fig. 9 (An example is shown here for the composition with x=1) show that the isotherms plotted of the form $M^2 = f(H/M)$ have positive slopes, for temperatures around T_C, which confirms that the magnetic transition from the ferromagnetic state to the paramagnetic state is of second order type.

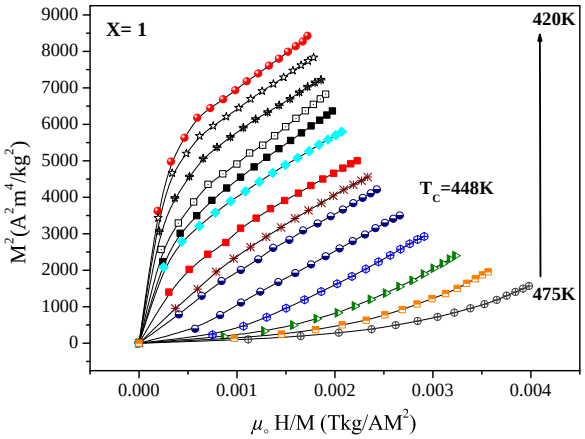

Figure 9. Isotherm magnetization curves, $M(H)$, for $Tb_2Fe_{17-x}Al_x$ compounds measured at different temperatures around the Curie temperature for magnetic fields between 0 and 1.5 T.

C. Magnetocaloric study

To assess how replacing iron with aluminum affects the magnetocaloric properties of $Tb_2Fe_{17-x}Al_x$ compounds, we calculated the magnetic entropy change ΔS_M as a function of temperature for various aluminum compositions. This was done by numerically integrating the $M(H)$ curves measured at different temperatures under an applied magnetic field of 1.5 T, using the equation presented in [33].

$$\Delta S_M = \int_0^H \left(\frac{\partial M}{\partial T}\right)_H dH$$

$$\Delta S_M \approx \sum_i \frac{1}{T_{i+1} - T_i} \left(M_{i+1} - M_i\right) \Delta H_i$$

In order to evaluate the potential of a magnetic material for use in magnetic refrigeration applications, it is important to assess its relative cooling power (RCP). The RCP is calculated by multiplying the peak value of the magnetic entropy change (ΔS_M) by the full width at half maximum (δT_{FWHM}) of ΔS_M. The equation used to determine RCP is provided by F. Fujita et al. in their paper [25].

$$RCP = -\Delta S_M \cdot \delta T_{\mathrm{FWHM}}$$

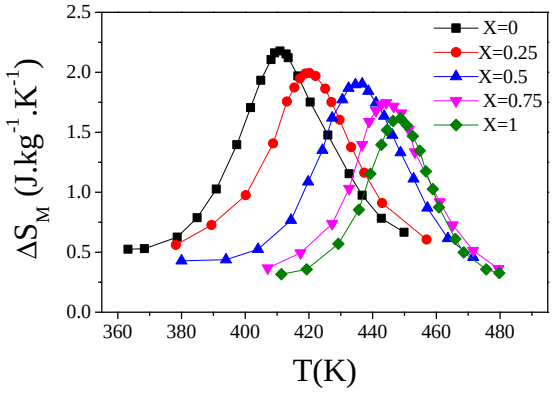

Figure 10. Magnetic entropy change $\Delta S(T, \mu_0 H)_{\mathrm{M}}$ for $Tb_2Fe_{17-x}Al_x$ samples.

Table II. Curie temperature, saturation magnetization, magnetic entropy maximum change and relative cooling power of $Tb_2Fe_{17-x}Al_x$ ($x = 0.25, 0.5, 0.75, 1$)

x(Al)	0	0.25	0.5	0.75	1
T_C (K)	412	421	437	445	448
M_s (Am^2/kg)	119.6	111.2	101.2	92.8	81.5
ΔS_M(J/kgK)	2.19	2.01	1.91	1.75	1.6
RCP (J/kg)	88	87	76	60	42

The magnetic entropy change change ΔS_M as a function of temperature for various compositions is illustrated in Fig.10. At the Curie temperature of each compound, the maximum magnetic entropy ΔS_M is clearly defined, and it slightly decreases as the aluminum content increases. For example, the maximum ΔS_M for the hexagonal structured $Tb_2Fe_{17-x}Al_x$ compounds is 2.19, 1.91, and 1.6 $Jkg^{-1}K^{-1}$ for aluminum contents x of 0, 0.5, and 1, respectively (Tab.II).

These ΔS_M values are similar to those reported for the Y_2Fe_{17} and Nd_2Fe_{17} systems [26]. However, a lower ΔS_M value was found for the rhombohedral crystal structure of Tb_2Fe_{17} [50]. Furthermore, a reduction in the peak width of the temperature dependence of ΔS_M is observed, which becomes more apparent with an increase in aluminum content. This reduction causes a decline in the relative cooling power (RCP) from 88 J/kg for $x = 0$ to 42 J/kg for $x = 1$ (Tab. II).

Aside from the Relative Cooling Power (RCP), another significant parameter employed to assess the suitability of materials for magnetic refrigeration technologies is the temperature-averaged entropy change (TEC). This additional figure of merit, introduced by L. D. Griffith *et al.* [51], can be computed utilizing magnetic entropy change data in the following manner:

$$TEC = \frac{1}{\Delta T_{H-C}} \max \left\{ \int_{T_{mid}-\frac{\Delta T_{H-C}}{2}}^{T_{mid}+\frac{\Delta T_{H-C}}{2}} |\Delta S_M(T)| dT \right\}$$

ΔT_{H-C} is characterized as the temperature range of the measuring device, signifying the disparity between the hot and cold heat exchangers. The temperature value denoted by T_{mid} corresponds to the midpoint of ΔT_{H-C}, which optimizes the Temperature-Averaged Entropy Change (TEC).

The Tab. III shows TEC values for $Tb_2Fe_{17-x}Al_x$ compounds with TEC values for other magnetocaloric oxide and intermetallic compounds. As the aluminum concentration increases, the normalized TEC ($\frac{TEC}{\Delta \mu_0 H}$) value appears to remain constant.

In comparison with other normalized TEC values, such as those listed in the table, the values of the $Tb_2Fe_{17-x}Al_x$ series are comparable to those of the compounds $Pr_{0.5}Er_{0.1}Sr_{0.4}MnO_3$, $Pr_{0.5}Eu_{0.1}Sr_{0.4}MnO_3$, Ho_2CoMnO_6, $La_{0.8}Ca_{0.05}Na_{0.15}MnO_3$, and $TmFe_{0.8}Mn_{0.2}O_3$. However, the normalized TEC of the compounds studied in this work is slightly lower than that of the intermetallic compound $Pr_{1.64}Sm_{0.36}Fe_{17}$. The $Tb_2Fe_{17-x}Al_x$ series of compounds exhibit a good magnetocaloric effect and a controllable operating temperature.

Table III. The TEC values of our sample and the TEC values of other materials are used for comparison.

Material	T_{mid}	$\Delta\mu_0 H$	ΔT_{H-C}	TEC	$\frac{TEC}{\Delta\mu_0 H}$	Ref
	K	T	K	$J(Kkg)^{-1}$	$J(KkgT)^{-1}$	
Tb_2Fe_{17}	410	1.5	5	1.48	0.98	this work
$Tb_2Fe_{16.75}Al_{0.25}$	420	1.5	5	1.44	0.96	this work
$Tb_2Fe_{16.5}$ $Al_{0.5}$	435	1.5	5	1.42	0.95	this work
$Tb_2Fe_{16.25}Al_{0.75}$	444.5	1.5	5	1.36	0.91	this work
$Tb_2Fe_{16}Al_1$	448.5	1.5	5	1.3	0.86	this work
$Pr_{0.5}Er_{0.1}Sr_{0.4}MnO_3$	188.5	5	5	4.9	0.98	[46]
$Pr_{0.5}Eu_{0.1}Sr_{0.4}MnO_3$	279.9	5	5	4.45	0.89	[46]
$La_{0.8}Ca_{0.05}Na_{0.15}MnO_3$	315	5	5	4.55	0.91	[47]
$La_{0.8}Na_{0.2}MnO_3$	330	5	5	4.6	0.92	[47]
Ho_2CoMnO_6	77	7	5	6.5	0.928	[48]
$TmFe_{0.8}Mn_{0.2}O_3$	12	7	5	6.4	0.914	[49]
$TmFe_{0.7}Mn_{0.3}O_3$	11	7	5	7	1	[49]
$Pr_{1.64}Sm_{0.36}Fe_{17}$	300	3	5	3.71	1.24	[5]

IV. CONCLUSION

In the present work, the structure and magnetic and magnetocaloric properties of the $Tb_2Fe_{17-x}Al_x$ compounds with $x = 0, 0.25, 0.5, 0.75$, and 1 were studied. These compounds are difficult to prepare by mechanosynthesis since several other phases appear; therefore, the compounds were elaborated by arc furnace without subsequent annealing. We have shown that the $Tb_2Fe_{17-x}Al_x$ compounds have a Th_2Ni_{17} hexagonal structure with a $P6_3/mmc$ space group. The Rietveld refinement of the X-ray diffractograms allowed determining the structural parameters for different amounts of aluminum. Lattice parameters and the unit cell volume increase with aluminum amounts while the c/a ratio remains nearly constant. The $Tb_2Fe_{17-x}Al_x$ compounds exhibit a second-order magnetic phase transition from a ferromagnetic state to a paramagnetic state. This transition is temperature-induced and takes place around the Curie temperature. The lattice parameters increase with aluminum content, and the same behavior is observed for T_C values. The saturation magnetization M_s decreases with the increase of aluminum content. The decrease is mainly due to magnetic dilution. Magnetic entropy and relative cooling power decrease as the aluminum amount increases. The $Tb_2Fe_{17-x}Al_x$ compounds are among the materials with a moderate magnetocaloric effect and a controllable operating temperature.

AUTHOR CONTRIBUTIONS

S. Charfeddine, I. Souid, and H. Jaballah: Investigation, Data Curation, Conceptualization, Writing - Original Draft, Writing - Review, Editing and Validation. L. Bessais and A. Korchef: Methodology, Writing - Review and Editing, Supervision, Project administration.

ACKNOWLEDGMENTS

This work is mainly supported by the Ministry of High Education, Scientific Research and Technology, University of Carthage, (Tunisia) and the ICMPE, CNRS, UMR 7182, Thiais, France.

Data availability

All data generated or analyzed during this study are included in this published article.

Funding

The authors did not receive support from any organization for the submitted work.

DECLARATIONS

Conflict of interest

The authors have no relevant financial or non-financial interests to disclose.

Competing interest

The authors have no competing interests to declare that are relevant to the content of this article.

Disclosure

The authors declare that they have no known competing financial interests or personal relationships that could have appeared to influence the work reported in this paper.

[1] A. Korchef, A.W. Kolsi, and N. Njah. *J. Mater. Sci.*, 42:5411–5415, 2007.

[2] K. Gschneidner, A. Russell, A. Pecharsky, J. Morris, Z. Zhang, and T. Lograsso. *Nature Mater.*, 2:587–591, 2003.

[3] K. Nouri, M. Saidi, S. Walha, L. Bessais, and M. Jemmali. *Chemistry Africa*, 3:111–118, 2020.

[4] V. Franco, J. S. Blázquez, J. J. Ipus, J. Y. Law, L. M. Moreno-Ramirez, and A. Conde. *Prog. Mater. Sci.*, 93:112–232, 2018.

[5] H. Jaballah, W. Bouzidi, R. Fersi, N. Mliki, and L. Bessais. *J. Phys. Chem*, 161:110438, 2021.

[6] Z. Ma, X. Dong, Z. Zhang, and L. Li. *J. Mater. Sci. Technol.*, 92:138–142, 2021.

[7] D. Guo, L.M. Moreno-Ramírez, C. Romero-Muñiz, Y. Zhang, J-Y. Law, V. Franco, J. Wang, and Z. Ren. *Sci. China Mater*, 64(11):2846–2857, 2021.

[8] H. Jaballah, V. Charbonnier, L. Bessais, and N. Mliki. *Mater. Res. Bull.*, page 112326, 2023.

[9] R. Guetari, R. Bez, A. Belhadj, K. Zehani, A. Bezergheanu, N. Mliki, L. Bessais, and C. B. Cizmas. *J. Alloys Compd.*, 588:64–69, 2014.

[10] W. Bouzidi, K. Nouri, T. Bartoli, R. Sedek, H. Lassri, J. Moscovici, and L. Bessais. *J. Magn. Magn. Mater.*, 497:166018, 2020.

[11] N. Bouchaala, M. Jemmali, T. Bartoli, K. Nouri, I. Hentech, S. Walha, L. Bessais, and A. Ben Salah. *journal of solid state chemistry*, 258:501–209, 2018.

[12] K. Umadevi, A. Talapatra, J. Arout Chelvane, M. Palit, J. Mohanty, and V. Jayalakshmi. *J. Appl. Phys.*, 122:065108, 2017.

[13] T. Bartoli, W. Bouzidi, FZ. Rachid, R. Moubah, H. Lassri, J. Moscovici, and L. Bessais. *J Mater Sci Mater Electron*, pages 1–8, 2022.

[14] M. Saidi, L. Bessais, and M. Jemmali. *J. Phys. Chem. Solids*, 160:110343, 2022.

[15] W. Bouzidi, K. Nouri, T. Bartoli, H. Jaballah, S. Ayadim, J. Moscovici, and L. Bessais. *Appl. Phys. A*, 128(7):566, 2022.

[16] H. Jaballah, K. Nouri, N. Mliki, L. Bessais, and M. Jemmali. *Chem. Phys. Lett.*, 787:139260, 2022.

[17] H. Jaballah, R. Guetari, N. Mliki, and L. Bessais. *J. Phys. Chem. Solids*, 169:110752, 2022.

[18] M. P. Dariel, J. T. Holthuis, and M. R. Pickus. *J. Less-Common. Met.*, 45:91–101, 1976.

[19] I. G. Orlova, A. A. Eliseev, G.E. Chuprikov, and F. Rukk. *Russ. J. Inorg. Chem.*, 22:1387–1389, 1977.

[20] S. Landin and J. Agren. *J. Alloys Compd.*, 207-208:449–453, 1994.

[21] H. Okamoto. *J. Phase Equilibria*, 17:80, 1996.

[22] K. H. J. Buschow. *Rep. Prog. Phys.* , 54:1123, 1991.

[23] K. Zehani, R. Guetari, N. Mliki, and L. Bessais. *Physics Procedia*, 75:1435–1441, 2015.

[24] S. Charfeddine, K. Zehani, L. Bessais, and A. Korchef. *J. Solid State Chem.*, 238:15–20, 2016.

[25] A. Fujita, S. Fujieda, and K. Fukamichi. *J. Magn. Magn. Mater.*, 321:3553–3558, 2009.

[26] P. Alavarez, P. Gorria, J. Sanchez-Llamazares, M.J. Perez, V.Franco, M.Reiffers, J. Kovac, I. Puente-Orench, and J. Blanco. *Mater. Chem. Phys.*, 2011.

[27] J. M. D Coey and H. Sun. *J. Magn. Magn. Mater.*, 87:L251–L254, 1990.

[28] Z. Sun, H. Zhang, J.Y. Wang, and B.G. Shen. *J. Appl. Phys.*, 86:5152, 1999.

[29] J. Pospisil, J.P. Vejpravova, D. Niznansky, and V. Sechovsky. *J. Magn. Magn. Mater.*, 310:629, 2007.

[30] Z W Li, X Z Zhou, and A H Morrish. *Phys. Rev. B*, 51:2891, 1995.

[31] Y.V. Sherbacova, G.E. Ivanova, N.V. Mushinkov, and I.V. Gervasera. *J. Alloys Compd.*, 308:15, 2000.

[32] T. Yanson, M. Manyakov, O. Bodak, R. Cerny, and K. Yvon. *J. Alloys Compd.*, 320:108–113, 2001.

[33] M. Foldeaki, R. Chahine, and T. K. Bose. *J. Appl. Phys.*, 77:3528, 1995.

[34] L. Bessais, S. Sab, C. Djega-Mariadassou, N. H. Dan, and N. X. Phuc. *Phys. Rev. B*, 70:134401, 2004.

[35] L. Bessais, E. Dorolti, and C. Djega-Mariadassou. *J. Appl. Phys.*, 97:013902, 2005.

[36] Z. Cheng, B. Shen, Q. Yan, H. Guo, D. Chen, C. Gou, K. Sun, F. R. de Boer, and K. H. J. Buschow. *Phys. Rev. B*, 57:14299–14309., 1998.

[37] S. R. Mishra, Gary J. Long, O. A. Pringle, D. P. Middleton, K. H. J. Buschow, and F. Grandjean. *J. Magn. Magn. Mater.*, 162:167–176, 1996.

[38] D. Givord and R. Lemaire. *IEEE Trans. Magn.*, 10:109, 1974.

[39] Z.W. Li and A. H. Morrish. *Phys. Rev. B.*, 55(6):3670, 1997.

[40] L. Bessais, C. Djega-Mariadasso, D.K. Tung, and W. Hong N.X. Phuc. *J. Alloys Compd.*, 455(1-2):35–41, 2008.

[41] Z. W. Li and X. A. H. Morrish. *Phys. Rev. B*, 55:3670–3676, 1997.

[42] K. Zehani, R. Bez, A. Boutahar, EK Hlil, H. Lassri, J. Moscovici, N. Mliki, and L. Bessais. *J. Alloys Compd.*, 591:58–64, 2014.

[43] E.M. Chudnovsky and R.A. Serota. *J. Phys. C*, 16:4181, 1983.

[44] H. Lassri and R. Krishnan. *J. Magn. Magn. Mater.*, 157:104–107, 1992.

[45] I. A. Al-Omari, Y. Yeshurun, S. S. Jaswal, and D. J. Sellmyer. *J. Magn. Magn. Mater.*, 208:93, 2000.

[46] A. Sakka, R. M'nassri, MM. Nofal, S. Mahjoub, W. Cheikhrouhou-Koubaa, N. Chniba-Boudjada, M. Oumezzine, and A. Cheikhrouhou. *J. Magn. Magn. Mater.*, 514:167158, 2020.

[47] S. Choura-Maatar, M.M. Nofal, R. Mnassri, W. Cheikhrouhou Koubaa, N. Chniba-Boudjada, and A. Cheikhrouhou. *J. Mater. Sci.: Mater. Electron.*, 31:1634–1645, 2020.

[48] D. Mazumdar and I. Das. *J. Appl. Phys.*, 129(6):063901, 2021.

[49] L. Su, X.Q. Zhang, Q.Y. Dong, H. T. Yangand S. H. Li, and Z. H. Cheng. *Ceram. Int*, 47(13):18286–18294, 2021.

[50] H. Chen, Y. Zhang, J. Han, H. Du, Ch. Wang, and Y. Yang. *J. Magn. Magn. Mater.*, 320:1382–1384, 2008.

[51] L. D. Griffith, Y. Mudryk, J. Slaughter, and V. K. Pecharsky. *Journal of Applied Physics*, 123(3):034902, 2018.